Sustainable Energy Technologies and Assessments 23 (2017) 1–10

Contents lists available at ScienceDirect

Sustainable Energy Technologies and Assessments

journal homepage: www.elsevier.com/locate/seta

Original article

A comparative study of Three–Phase Dual Active Bridge Converters for renewable energy applications

R.O. Núñez [a,b,*], G.G. Oggier [b], F. Botterón [a], G.O. García [b]

[a] Grupo de Investigación y Desarrollo en Ingeniería Electrónica (GID-IE)-IMAM-CONICET, Facultad de Ingeniería, Universidad Nacional de Misiones (UNaM), Juan Manuel de Rosas #325, 3365BOG Oberá, Misiones, Argentina

[b] Grupo de Electrónica Aplicada (GEA), Facultad de Ingeniería, Universidad Nacional de Río Cuarto (UNRC), CONICET, Ruta Nacional #36 Km. 601, X5804BYA Río Cuarto, Córdoba, Argentina.

ARTICLE INFO

Article history:
Received 30 May 2016
Revised 25 June 2017
Accepted 17 July 2017

Keywords:
Renewable energy sources
Energy efficiency
Energy storage
DC–DC bidirectional converters
Three–phase dual active bridges
Soft switching
Three–phase transformers

ABSTRACT

The influence of different transformers in the operation of a three–phase dual active bridges DC–DC converter is analyzed. The transformers considered have their windings connected in star–star, delta–delta, star–delta and delta–star. The main objective of this paper is to obtain factors of merits to allow the selection of a transformer which will yield higher converter performance for a given application. These factors of merits allows estimate the losses in power semiconductors and high frequency transformers. Additionally, operation regions under soft switching are deduced for each transformer.

Introduction

The technological advance in various fields of application renewed the interest in using DC power. This created a need for power electronics converters to satisfy different specifications.

In some hybrid energy conversion systems, such as microgrids with high green energy penetration (wind, photovoltaic, biogas), hybrid vehicles, uninterruptible power supply, among other applications; power storage units such as banks of batteries and supercapacitors are used [1–9]. The power exchange between these storage units and the rest of the system must be performed through bidirectional DC–DC converters aiming to control de energy flux in both directions and to adapt different levels of voltages [10–12]. The Dual Active Bridges DC–DC Converters (DABC) are an interesting choice in these applications [13–16].

There are several published works concerning Single–Phase Dual Active Bridges Converters (SPDABC) [17–20] and Three–Phase Dual Active Bridges Converters (TPDABC) [14,21–25]. The latter are more frequently used when a higher density of power is needed.

In [14,26,27] some advantages of TPDABC are shown in opposition to SPDABC, among which the most relevant are lower peak current in power semiconductors, lower effective current in filters and a higher usage factor in the transformer.

Aiming to reduce losses with power semiconductors in TPDABC, there are different suggestions, such as adding auxiliary circuits [22,23] and/or using different modulation strategies [24,25].

This text widens the analysis presented previously in [28–32], related to the impact of high frequency transformers, with different individual connections: YY, ΔΔ, YΔ and ΔY, which allows different TPDABC configurations. Factors of merit are defined both in transformers and power semiconductors, for each of the mentioned configurations. Additionally, analysis and assessment of operation region limits with soft commuting of power semiconductors. According to the factors mentioned, a comparison is made to determine the advantages and disadvantages of each configuration.

This work is organized as follows: In Section "Principle of operation and analysis of the TPDABC" the TPDABC principle of operation is presented and described. In Section "Evaluation of the transformer rms current and VA_{Rating}", the transformer rms currents and transformer VA_{Rating} are evaluated. In Section "Evaluation of

* Corresponding author at: Grupo de Investigación y Desarrollo en Ingeniería Electrónica (GID-IE)-IMAM-CONICET, Facultad de Ingeniería, Universidad Nacional de Misiones (UNaM), Juan Manuel de Rosas #325, 3365BOG Oberá, Misiones, Argentina.

E-mail address: nunez.ruben.o@gmail.com (R.O. Núñez).

http://dx.doi.org/10.1016/j.seta.2017.07.004
2213-1388/

stress in the Power semiconductors" the stress on the power semiconductors are analyzed. The soft–switching operation regions' limits are determined in Section "Determination of soft–switching operation regions". In Section "Comparison and discussion of the results" the TPDABC configurations' performance are compared. Finally, conclusions are drawn in Section "Conclusions".

Principle of operation and analysis of the TPDABC

The topology of the TPDABC is presented in Fig. 1. The TPDABC is a dc–dc bidirectional converter able to operate as boost or buck converter. The topology consists of two three–phase active bridges, represented by B_1 and B_2 in Fig. 1. Both active bridges are composed of three legs of power semiconductors, which generate each line voltage at each side of a high–frequency three–phase transformer, T_x. These active bridges operate as either inverters or rectifiers, depending on the power flow direction.

Power transfer is controlled through the phase–shift modulation between the homologous voltages on both sides of the three–phase transformer.

To facilitate the analysis of the TPDABC operating principle, all the variables and parameters are referred to one side of the transformer and the transformer turn ratio is considered unitary (n= 1). In addition, high magnetizing inductances are considered, so that they may be neglected in this analysis. The winding resistances are also neglected due to its low values. This allows a simplified representation of the transformer by means of an equivalent circuit composed by only one inductance per phase, that represents the sum of the leakage inductances at both sides of the transformer.

Four different three–phase transformers, with star–star (YY), delta–delta (ΔΔ), star–delta (YΔ) and delta–star (ΔY) connections, are considered as part of the TPDABC, giving place to the following different configurations: TPDABCYY, TPDABCΔΔ, TPDABCYΔ and TPDABCΔY, respectively.

The methodology used to analyze the operation principle of the TPDABC is similar to that presented in [14], where TPDABCYY is analyzed, based on the study of ideal voltages and current waveforms of each transformer phase.

Fig. 2 shows the main ideal voltages and currents waveforms for the different configurations evaluated in this work. In this figure, for each of the configurations, different conduction intervals of the phase currents have been defined. It can be observed, in the same figure, that for TPDABCYY and TPDABCΔΔ configurations, six different current conduction intervals are defined whereas fiver intervals are defined for TPDABCYΔ and TPDABCΔY.

Analyzing the current waveform flowing through the leakage inductance of each phase, its analytical expression can be obtained for the intervals defined above as a function of $\theta = \omega t$; where $\omega = 2\pi f_s$, f_s is the switching frequency and t is time.

Depending on the phase shift between homologous voltages at each side of the three–phase transformer, ϕ, it can be demonstrated that the currents can be represented by two equations systems, for each configuration [28–30]. As an example, one of the two equation systems corresponding to each of the configurations analyzed is presented in Tables 1–3. The other equation system has not been included in this work in order to avoid using too much space.

In these tables, considering that $n = 1$, d represents the converter voltage conversion ratio, defined as:

$$d = \frac{V_2}{V_1}, \tag{1}$$

where V_1 is the dc voltage of bridge B_1 and V_2 is the dc voltage of bridge B_2. It operates in buck mode when $d < 1$ and in boost mode when $d > 1$ [16].

The methodology used to determine the average power transferred by the converter is presented below. First, it is assumed that the average value of current waveforms in steady state is zero,

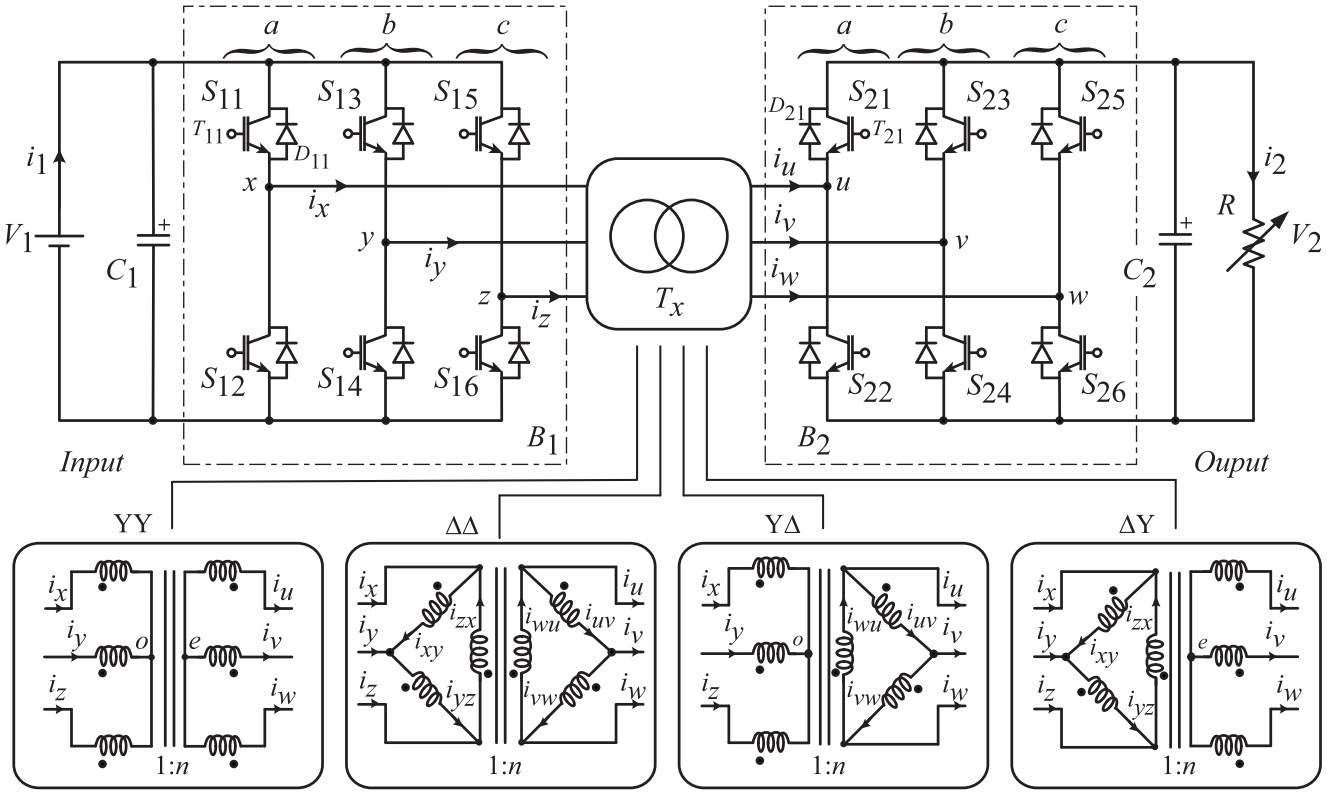

Fig. 1. Representation of the Three–Phase Dual Active Bridge Converter.

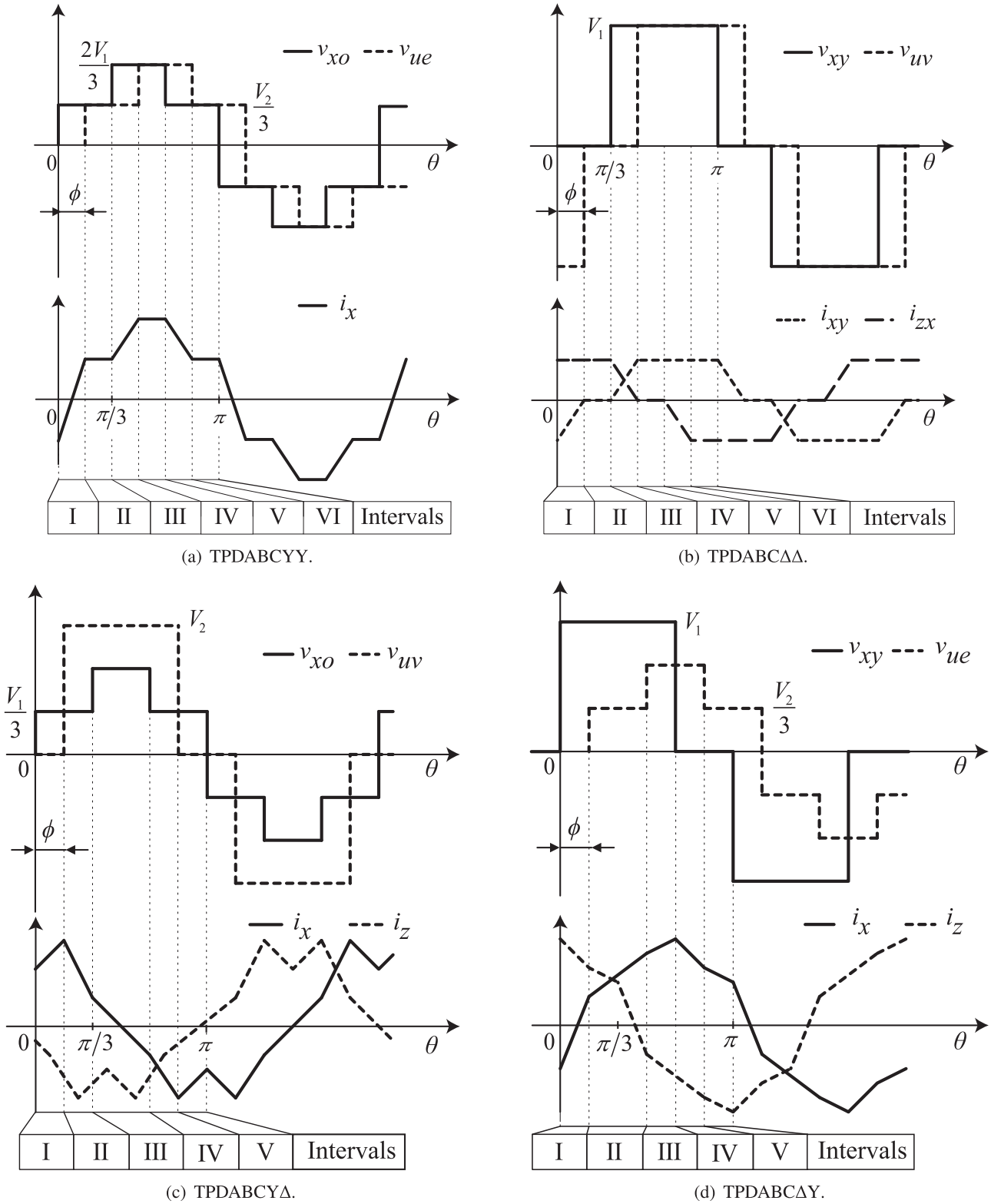

Fig. 2. Ideal waveforms for different configurations of the TPDABC. Voltage (up) and currents (down) at each transformer phase.

which means that the following relation is satisfied: $i(0) = -i(\pi)$. This relation allows obtaining the value of current at angle 0° and therefore calculating the currents for each transformer phase, within the conduction interval. Once the current at each transformer phase has been obtained, the line currents and then the average current are calculated at the converter output, I_2. Multiplying I_2 by the output voltage, V_2, the expressions of the transferred power, P, for each configuration is finally obtained, as shown in Table 4.

From the expressions of the transferred power, it can be concluded that the sign and magnitude of ϕ, determine the flow direction and magnitude of the transferred power.

Table 1
Analytical representation of the transformer phase currents, corresponding to the intervals defined in Fig. 2, for TPDABCYY) and TPDABCΔΔ configurations.

Interval	TPDABCYY	TPDABCΔΔ
I: $(0 \leqslant \theta \leqslant \phi)$	$i_{YY}(\theta) = i(0) + k_1(1+d)\theta$	$i_{\Delta\Delta}(\theta) = i(0) + k_2 d\theta$
II: $(\phi \leqslant \theta \leqslant \frac{\pi}{3})$	$i_{YY}(\theta) = i_{YY}(\phi) + k_1(1-d)(\theta-\phi)$	$i_{\Delta\Delta}(\theta) = i_{\Delta\Delta}(\phi)$
III: $(\frac{\pi}{3} \leqslant \theta \leqslant \frac{\pi}{3}+\phi)$	$i_{YY}(\theta) = i_{YY}(\frac{\pi}{3}) + k_1(2-d)(\theta-\frac{\pi}{3})$	$i_{\Delta\Delta}(\theta) = i_{\Delta\Delta}(\frac{\pi}{3}) + k_2(\theta-\frac{\pi}{3})$
IV: $(\frac{\pi}{3}+\phi \leqslant \theta \leqslant \frac{2\pi}{3})$	$i_{YY}(\theta) = i_{YY}(\frac{\pi}{3}+\phi) + 2k_1(1-d)(\theta-\phi-\frac{\pi}{3})$	$i_{\Delta\Delta}(\theta) = i_{\Delta\Delta}(\frac{\pi}{3}+\phi) + k_2(\theta-\frac{\pi}{3}-\phi)$
V: $(\frac{2\pi}{3} \leqslant \theta \leqslant \frac{2\pi}{3}+\phi)$	$i_{YY}(\theta) = i_{YY}(\frac{2\pi}{3}) + k_1(1-2d)(\theta-\frac{2\pi}{3})$	
VI: $(\frac{2\pi}{3}+\phi \leqslant \theta \leqslant \pi)$	$i_{YY}(\theta) = i_{YY}(\frac{2\pi}{3}+\phi) + k_1(1-d)(\theta-\frac{2\pi}{3}-\phi)$	
$i(0)$:	$k_1(\frac{2\pi d}{3} - \phi d - \frac{2\pi}{3})$	$k_2(\pi d - 6\phi d - \pi)$

where: $i(0)$ = initial condition of the currents, $k_1 = V_1/3\omega L_{YY}$ and $k_2 = V_1/3\omega L_{\Delta\Delta}$.

Table 2
Analytical representation of the transformer phase currents, corresponding to the intervals defined in Fig. 2, for TPDABCΔY configuration.

Interval	TPDABCYΔ
I: $(0 \leqslant \theta \leqslant \phi)$	$i_{Y\Delta}(\theta) = i(0) + k_3\theta$
II: $(\phi \leqslant \theta \leqslant \frac{\pi}{3})$	$i_{Y\Delta}(\theta) = i_{Y\Delta}(\phi) + k_3(1-3d)(\theta-\phi)$
III: $(\frac{\pi}{3} \leqslant \theta \leqslant \frac{2\pi}{3})$	$i_{Y\Delta}(\theta) = i_{Y\Delta}(\frac{\pi}{3}) + k_3(2-3d)(\theta-\frac{\pi}{3})$
IV: $(\frac{2\pi}{3} \leqslant \theta \leqslant \frac{2\pi}{3}+\phi)$	$i_{Y\Delta}(\theta) = i_{Y\Delta}(\frac{2\pi}{3}) + k_3(1-3d)(\theta-\frac{2\pi}{3})$
V: $(\frac{2\pi}{3}+\phi \leqslant \theta \leqslant \pi)$	$i_{Y\Delta}(\theta) = i_{Y\Delta}(\frac{2\pi}{3}+\phi) + k_3(\theta-\frac{2\pi}{3}-\phi)$
$i(0)$:	$k_3\pi(d-\frac{2}{3})$

where: $i(0) =$ initial condition of the current and $k_3 = \frac{V_1}{3\omega L_{Y\Delta}}$.

Table 3
Analytical representation of the transformer phase currents, corresponding to the intervals defined in Fig. 2, for TPDABCΔY configuration.

Interval	TPDABCΔY
I: $(0 \leqslant \theta \leqslant \phi)$	$i_{\Delta Y}(\theta) = i(0) + k_4(3+d)\theta$
II: $(\phi \leqslant \theta \leqslant \frac{\pi}{3}+\phi)$	$i_{\Delta Y}(\theta) = i_{\Delta Y}(\phi) + k_4(3-d)(\theta-\phi)$
III: $(\frac{\pi}{3}+\phi \leqslant \theta \leqslant \frac{2\pi}{3})$	$i_{\Delta Y}(\theta) = i_{\Delta Y}(\frac{\pi}{3}+\phi) + k_4(3-2d)(\theta-\phi-\frac{\pi}{3})$
IV: $(\frac{2\pi}{3} \leqslant \theta \leqslant \frac{2\pi}{3}+\phi)$	$i_{\Delta Y}(\theta) = i_{\Delta Y}(\frac{2\pi}{3}) - 2k_4 d(\theta-\frac{2\pi}{3})$
V: $(\frac{2\pi}{3}+\phi \leqslant \theta \leqslant \pi)$	$i_{\Delta Y}(\theta) = i_{\Delta Y}(\frac{2\pi}{3}+\phi) - k_4 d(\theta-\frac{2\pi}{3}-\phi)$
$i(0)$:	$k_4(\frac{2}{3}\pi d - \pi - d\phi)$

where: $i(0)$ =initial condition of the current and $k_4 = \frac{V_1}{3\omega L_{\Delta Y}}$.

With the aim to compare the different evaluated configurations, its maximum power has to be the same. Therefore, it is necessary to determine the equivalent leakage inductances for each case, resulting in the following equalities,

$$L_{YY} = \frac{L_{\Delta\Delta}}{3} = \frac{L_{Y\Delta}}{\sqrt{3}} = \frac{L_{\Delta Y}}{\sqrt{3}}, \tag{2}$$

where L_{YY}, $L_{\Delta\Delta}$, $L_{Y\Delta}$ and $L_{\Delta Y}$, are the equivalent leakage inductances needed for the transformers connected in YY, ΔΔ, YΔ and ΔY, respectively.

Evaluation of the transformer rms current and VA_{Rating}

In this work all the obtained expressions are plotted in p.u., for which the following base values are defined: base voltage: $V_b = V_1$, base current: $I_b = V_1/(\omega L_{YY})$, and base power: $P_b = V_b I_b = V_1^2/(\omega L_{YY})$.

With the purpose of comparing the different TPDABC configurations, some factors of merit related with the transformer are defined as follows.

Evaluation of the rms transformer phase current

The rms transformer phase current, $i(\theta)$, can be calculated as follows:

Table 4
Power and stress of the power semiconductors in TPDABC.

Configuration	Phase shift	P	$I_{T_{rms}}$	VA_{Rating}	$\sum I_{rms}$	$\sum I_{sw}$
TPDABCYY	$0 \leqslant \phi \leqslant \frac{\pi}{3}$	$\frac{V_1^2}{\omega L_{YY}} d\phi\left(\frac{2}{3} - \frac{\phi}{2\pi}\right)$	$\frac{V_1}{\sqrt{243}\pi\omega L_{YY}} r_1$	$\frac{\sqrt{2}V_1^2}{\sqrt{243}\pi\omega L_{YY}} r_1$	$\frac{2V_1}{\sqrt{243}\pi\omega L_{YY}} r_1$	$\left\lvert\frac{2V_1}{9\omega L_{YY}}\right\rvert p_1$
	$\frac{\pi}{3} \leqslant \phi \leqslant \frac{2\pi}{3}$	$\frac{V_1^2}{\omega L_{YY}} d\left(\phi - \frac{\phi^2}{\pi} - \frac{\pi}{18}\right)$	$\frac{V_1}{\sqrt{243}\pi\omega L_{YY}} r_2$	$\frac{\sqrt{2}V_1^2}{\sqrt{243}\pi\omega L_{YY}} r_2$	$\frac{2V_1}{\sqrt{243}\pi\omega L_{YY}} r_2$	$\left\lvert\frac{2V_1}{9\omega L_{YY}}\right\rvert p_2$
TPDABCΔΔ	$0 \leqslant \phi \leqslant \frac{\pi}{3}$	$\frac{V_1^2}{\omega L_{\Delta\Delta}} d\phi\left(2 - \frac{3\phi}{2\pi}\right)$	$\frac{V_1}{9\sqrt{\pi}\omega L_{\Delta\Delta}} r_1$	$\sqrt{\frac{2}{27\pi}}\frac{V_1}{\omega L_{\Delta\Delta}} r_1$	$\frac{6V_1}{\sqrt{243}\pi\omega L_{\Delta\Delta}} r_1$	$\left\lvert\frac{2V_1}{3\omega L_{\Delta\Delta}}\right\rvert p_1$
	$\frac{\pi}{3} \leqslant \phi \leqslant \frac{2\pi}{3}$	$\frac{V_1^2}{\omega L_{\Delta\Delta}} d\left(3\phi - \frac{3\phi^2}{\pi} - \frac{\pi}{6}\right)$	$\frac{V_1}{9\sqrt{\pi}\omega L_{\Delta\Delta}} r_2$	$\sqrt{\frac{2}{27\pi}}\frac{V_1}{\omega L_{\Delta\Delta}} r_2$	$\frac{6V_1}{\sqrt{243}\pi\omega L_{\Delta\Delta}} r_2$	$\left\lvert\frac{2V_1}{3\omega L_{\Delta\Delta}}\right\rvert p_2$
TPDABCYΔ	$0 \leqslant \phi \leqslant \frac{\pi}{3}$	$\frac{V_1^2}{\omega L_{Y\Delta}} d\left(\phi - \frac{\pi}{6}\right)$	$\frac{V_1}{\sqrt{243}\,\omega L_{Y\Delta}} m_1$	$\frac{\sqrt{2}(3d+\sqrt{3})V_1^2}{54\,\omega L_{Y\Delta}} m_1$	$\frac{(\sqrt{3}+3)V_1}{27\,\omega L_{Y\Delta}} m_1$	$\left\lvert\frac{2V_1}{3\omega L_{Y\Delta}}\right\rvert g_1$
	$\frac{\pi}{3} \leqslant \phi \leqslant \frac{2\pi}{3}$	$\frac{V_1^2}{\omega L_{Y\Delta}} d\left(\frac{3\phi^2}{2\pi} - 2\phi - \frac{\pi}{3}\right)$	$\frac{V_1}{\sqrt{243}\pi\omega L_{Y\Delta}} m_2$	$\frac{\sqrt{2}(\sqrt{3}d+\sqrt{3})V_1^2}{54\sqrt{\pi}\,\omega L_{Y\Delta}} m_2$	$\frac{(\sqrt{3}+3)V_1}{27\sqrt{\pi}\,\omega L_{Y\Delta}} m_2$	$\left\lvert\frac{2V_1}{3\omega L_{Y\Delta}}\right\rvert g_2$
TPDABCΔY	$-\frac{\pi}{3} \leqslant \phi \leqslant 0$	$\frac{V_1^2}{\omega L_{\Delta Y}} d\left(\phi + \frac{\pi}{6}\right)$	$\frac{V_1}{\sqrt{243}\,\omega L_{\Delta Y}} j_1$	$\frac{\sqrt{2}(\sqrt{3}d+3)V_1^2}{54\,\omega L_{\Delta Y}} j_1$	$\frac{(3+\sqrt{3})V_1}{27\,\omega L_{\Delta Y}} j_1$	$\left\lvert\frac{2V_1}{3\omega L_{\Delta Y}}\right\rvert q_1$
	$0 \leqslant \phi \leqslant \frac{\pi}{3}$	$\frac{V_1^2}{\omega L_{\Delta Y}} d\left(\phi - \frac{3\phi^2}{2\pi} + \frac{\pi}{6}\right)$	$\frac{V_1}{\sqrt{243}\pi\omega L_{\Delta Y}} j_2$	$\frac{\sqrt{3}(\sqrt{2}d+\sqrt{6})V_1^2}{54\sqrt{\pi}\,\omega L_{\Delta Y}} j_2$	$\frac{(\sqrt{3}+3)V_1}{27\sqrt{\pi}\,\omega L_{\Delta Y}} j_2$	$\left\lvert\frac{2V_1}{3\omega L_{\Delta Y}}\right\rvert q_2$

where :

$r_1 = \sqrt{\pi^3\left(5d^2 - 10d + 5\right) + d\left(-27\phi^3 + 54\phi^2\pi\right)}$, $r_2 = \sqrt{\pi^3\left(5d^2 - 9d + 5\right) + d\left(-54\phi^3 + 81\phi^2\pi - 9\phi\pi^2\right)}$,

$m_1 = \sqrt{\pi^2\left(15d^2 - 15d + 5\right) + d\left(81\phi^2 - 27\phi\pi\right)}$, $m_2 = \sqrt{\pi^3\left(15d^2 - 12d + 5\right) + d\left(-81\phi^3 + 162\phi^2\pi - 54\phi\pi^2\right)}$,

$j_1 = \sqrt{\pi^2\left(5d^2 - 15d + 15\right) + d\left(81\phi^2 + 27\phi\pi\right)}$, $j_2 = \sqrt{\pi^3\left(5d^2 - 15d + 15\right) + d\left(-81\phi^3 + 81\phi^2\pi + 27\phi\pi^2\right)}$,

$p_1 = |2\pi + d(3\phi - 2\pi)| + |3\phi + 2\pi(d-1)|$, $p_2 = |2\pi + d(6\phi - 3\pi)| + |6\phi + \pi(2d-3)|$,

$g_1 = \pi(|d - \frac{2}{3}| + |2d - 1|)$, $g_2 = |\frac{2\pi}{3} + d(3\phi - 2\pi)| + |3\phi + 2\pi(d-1)|$,

$q_1 = \pi(|d-2| + |\frac{2d}{3} - 1|)$, $q_2 = |2\pi + d(3\phi - \pi)| + |3\phi + \pi(\frac{2d}{3} - 1)|$.

$$I_{rms} = \sqrt{\frac{1}{2\pi}\int_0^{2\pi} i^2(\theta)d\theta}, \quad (3)$$

where angle 2π represents a switching period.

From (3) and the current expressions given in Tables 1–3, the rms transformer phase current can be obtained, $I_{T_{rms}}$, for all ϕ intervals and for each converter configuration, as shown in Table 4.

In Fig. 3(a) the rms transformer phase current for each converter configuration have been plotted as functions of the output average current, for different values of d. It can be concluded that the configuration with the lowest rms current, for the converter operating at buck mode and for a wide range of output average current, is TPDABCYΔ; whereas for the converter operating at boost mode, the configuration with the lowest rms current value is TPDABCΔY.

Evaluation of the transformer VA_{Rating}

To calculate the transformer VA_{Rating}, the following expression is proposed [33]:

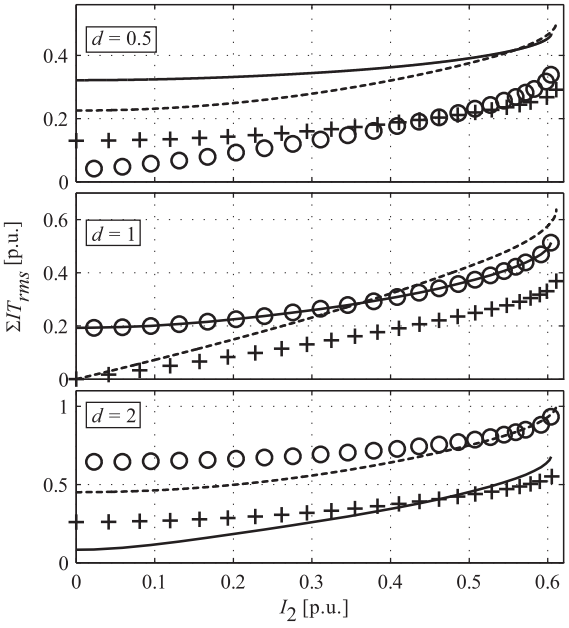

(a) Tranformer rms phase current.

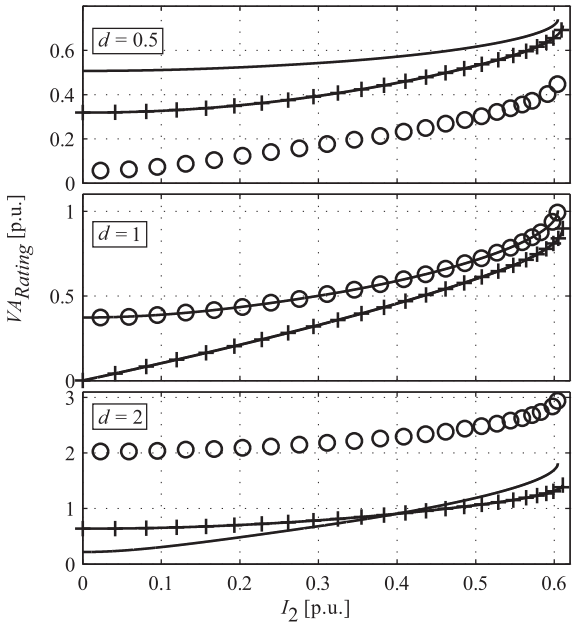

(b) Tranformer VA_{Rating}.

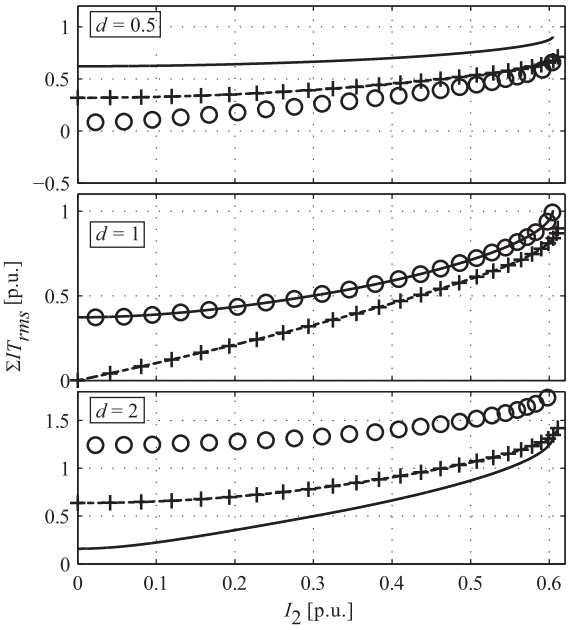

(c) Summation of the rms currents in the power semiconductors of both bridges corresponding to one phase of the converter.

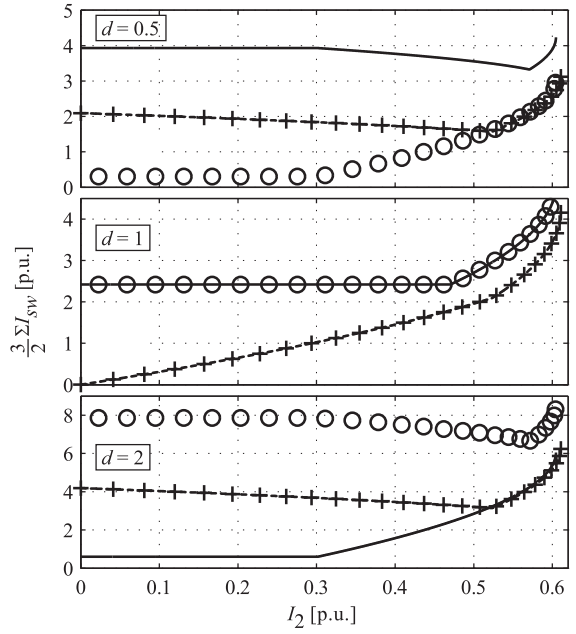

(d) Summation of the currents in the power semiconductors, at the switching instants, of both bridges corresponding to one phase of the converter.

Fig. 3. Evaluation of the transformer and semiconductors stress as functions of the output average current for different values of d. TPDABCYY: dash-dotted line; TPDABCΔΔ: plus symbol; TPDABCYΔ: circle line; TPDABCΔY: dashed line.

$$VA_{Rating} = 3\left(\frac{V_{T_{1rms}} I_{T_{1rms}} + V_{T_{2rms}} I_{T_{2rms}}}{2}\right). \quad (4)$$

where $V_{T_{1rms}}$, $I_{T_{1rms}}$ and $V_{T_{2rms}}$, $I_{T_{2rms}}$ pairs are the rms phase voltage and current in both sides of the transformer.

The rms phase voltage for the transformer connected in Y and Δ, based on V_1, can be calculated as follows:

For the windings connected in Y:

$$V_{Y_{rms}} = \frac{\sqrt{2}}{3} V_1, \quad (5)$$

For the windings connected in Δ:

$$V_{\Delta_{rms}} = \sqrt{\frac{2}{3}} V_1. \quad (6)$$

The analytical expressions that represent the transformer VA_{Rating} for each converter configuration can be determined by substituting the previous expressions of the rms voltage and current in (4), that are shown in Table 4.

In the Fig. 3(b) the transformer VA_{Rating} has been plotted as function of I_2 for different values of d. From this figure, it can be observed that when the converter operates in buck mode, the transformer VA_{Rating} is lower in the TPDABCYΔ, for the entire current operating range, whereas it is lower for TPDABCΔY operating in boost mode.

Table 5
Conditions to operate the TPDABC under soft–switching mode.

Leg	Bridge B_1	Bridge B_2
a	$i_x(\pi) \geqslant 0$	$i_u(\phi) \geqslant 0$
b	$i_y(\pi - \frac{2\pi}{3}) \geqslant 0$	$i_v(\phi - \frac{2\pi}{3}) \geqslant 0$
c	$i_z(\pi - \frac{4\pi}{3}) \geqslant 0$	$i_w(\phi - \frac{4\pi}{3}) \geqslant 0$

Evaluation of stress in the Power semiconductors

To evaluate the stress in the power semiconductors, the rms current value that flow through the semiconductors are calculated as a factor of merit related with the conducting losses. Moreover, the summation of the current values that flow through the semiconductors at the switching angles are calculated as factor of merit related with the switching losses. These factors allow the comparation of the different TPDABC configurations.

Evaluation of rms current in the power semiconductors

The conduction losses in power semiconductors are functions of the square values of the rms current flowing through them [34]. To estimate these losses, for the different configurations analyzed in this paper, a factor of merit, $\sum I_{rms}$, is defined in this subsection. This factor of merit is calculated by summing the expressions of the converter rms phase current flowing through the semiconductors of each bridge. An increase in this factor means an increase in the semiconductors power conduction losses.

The analytical expressions of line currents, $i_x(\theta)$ and a $i_u(\theta)$, can be used in Eq. (3) to calculate its rms value.

The cited factor calculations for each TPDABC configuration are shown in Table 4 and they are plotted in Fig. 3(c) as function of the average output current for different values of d. From this figure it can be concluded that for a wide range of the output average

Table 6
Limits of the soft–switching regions for different TPDABDC configurations.

Configuration of the converter	Interval 1		Interval 2	
	Bridge B_1	Bridge B_2	Bridge B_1	Bridge B_2
TPDABCYY – TPDABCΔΔ	$I_2 \leqslant \frac{2\pi}{9}\left(1 - \frac{1}{d^2}\right)$	$I_2 \geqslant \frac{2\pi}{9}\left(1 - d^2\right)$	$I_2 \leqslant \frac{\pi}{324}\left(63 - \frac{36}{d^2}\right)$	$I_2 \geqslant \frac{\pi}{36}\left(4d^2 - 7\right)$
TPDABCYΔ	$d \leqslant \frac{2}{3}$	$d \geqslant \frac{1}{2}$	$I_2 \leqslant \frac{\sqrt{3}\pi}{81}\left(9 - \frac{2}{d^2}\right)$	$I_2 \geqslant \frac{\sqrt{3}\pi}{9}\left(1 - 2d^2\right)$
TPDABCΔY	$d \leqslant 2$	$d \geqslant \frac{3}{2}$	$I_2 \leqslant \frac{\sqrt{3}\pi}{9}\left(1 - \frac{2}{d^2}\right)$	$I_2 \geqslant \frac{\sqrt{3}\pi}{81}\left(9 - 2d^2\right)$

For the configurations TPDABCYY and TPDABCΔΔ, the intervals 1 and 2 are limited by $0 \leqslant I_2 \leqslant 0.524$ and $0.524 \leqslant I_2 \leqslant 0.611$, respectively, whereas for configurations TPDABCYΔ and TPDABCΔY, these intervals are limited by $0 \leqslant I_2 \leqslant 0.302$ and $0.302 \leqslant I_2 \leqslant 0.605$, respectively.

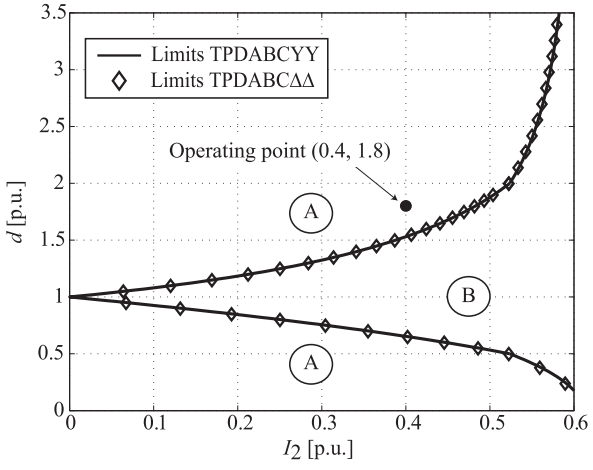

(a) Configurations TPDABCYY and TPDABCΔΔ: (A) hard switching and (B) soft switching.

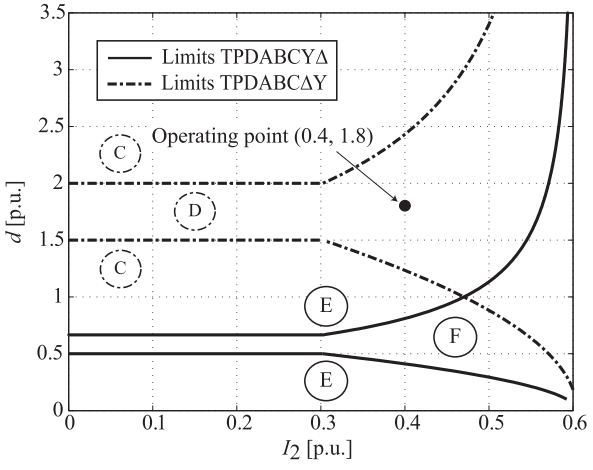

(b) Configurations TPDABCYΔ: (E) hard switching and (F) soft switching; TPDABCΔY: (C) hard switching and (D) soft switching.

Fig. 4. Soft–switching operation regions as functions of relation between the voltage and the output average current.

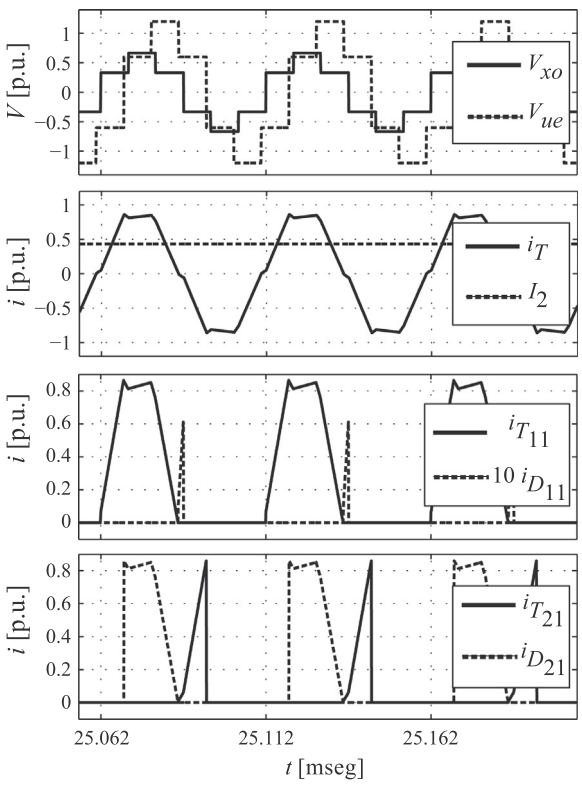

(a) TPDABCYY.

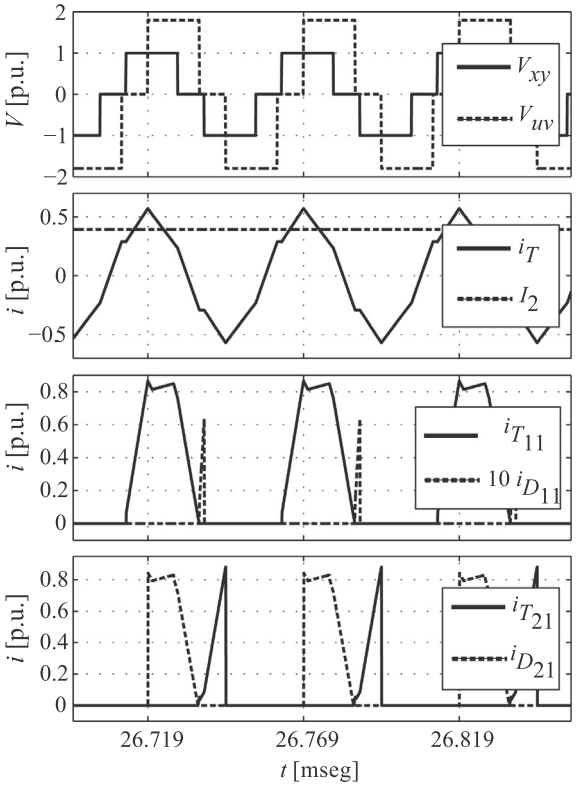

(b) TPDABCΔΔ.

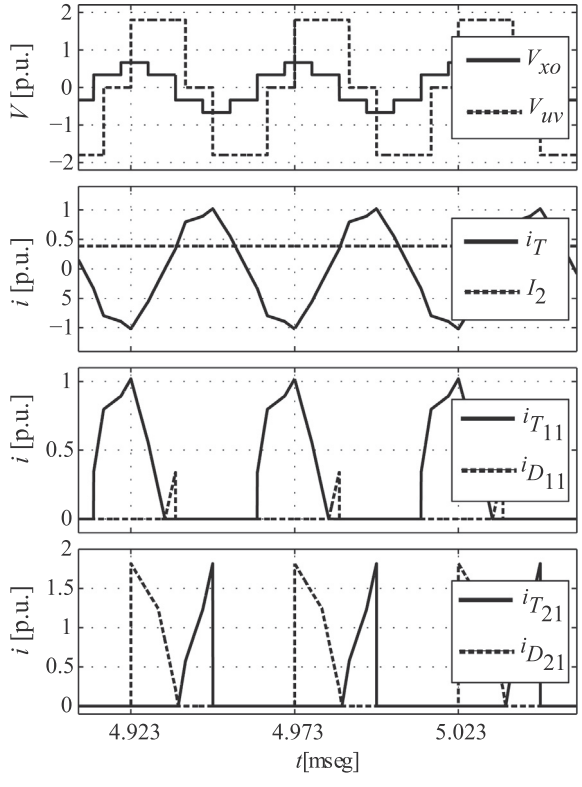

(c) TPDABCYΔ.

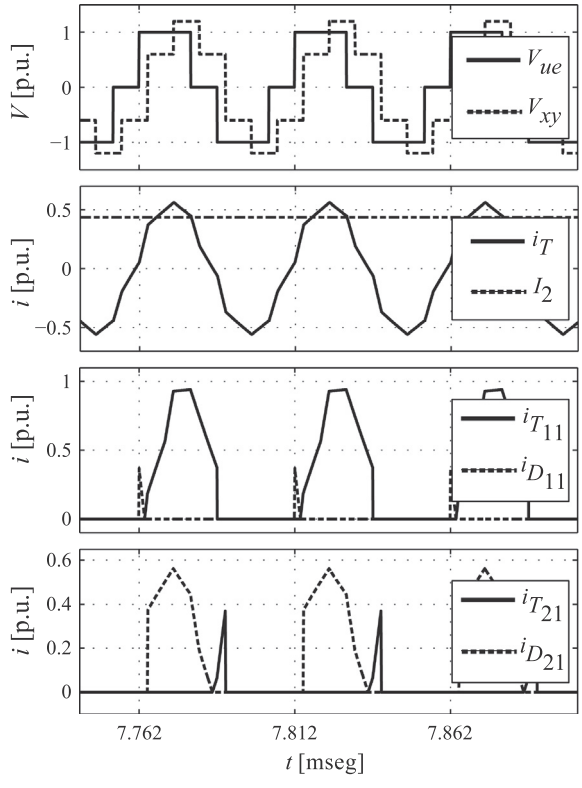

(d) TPDABCΔY.

Fig. 5. Simulation results for the operating point depicted in Fig. 4, given by $I_2 = 0.4$ p.u. and d=1.8.

current, when the values of $d < 1$ (buck mode of operation), the rms currents are smaller in the TPDABCYΔ configuration, whereas for values of $d > 1$ (boost mode of operation), they are lower for TPDABCYY configuration.

Evaluation of the summation of currents at the switching angles

Since to switching losses in the power semiconductors are functions of the current value flowing through them at the switching angles [34], this paper proposed the evaluation of the summation of these currents in both bridges as a factor of merit related with these losses.

This factor of merit for the different configurations is shown in Table 4 and they are plotted as functions of the output average currents, for different values of d in Fig. 3(d).

In Fig. 3(d), it can be observed that for $(d < 1)$, this factor is lower for a wider range of output average current in the TPDABCYΔ configuration. When $d > 1$ the switching losses are lower in the TPDABCΔY.

Determination of soft–switching operation regions

A strategy to reduce semiconductors' switching losses consists in operating the converter under soft–switching mode [34,35].

The conditions to operate the TPDABC under soft–switching mode are shown in Table 5 [14]. When these constrain are not fulfilled, the converter operates under hard–switching mode.

In the following, the limits for soft–switching operation are determined and compared for each TPDABC configuration.

By evaluating the inequalities shown in Table 5, the limits of the soft–switching regions for both bridges $(B_1 - B_2)$ and for each configuration considered in this work can be determined, which are presented in Table 6.

By analyzing the expressions in Table 6, it can be concluded that for TPDABCYΔ and TPDABCΔY configurations, when operating within interval 1, the soft–switching operation conditions are non–dependent of I_2, whereas in interval 2, the limits are function of I_2.

The limits of the soft–switching operation regions for the analyzed configurations are shown in Fig. 4.

In Fig. 4(a), it can be observed that the TPDABCYY and TPDABCΔΔ configurations can operate under soft switching mode in the whole range of I_2 only when $d = 1$.

From Fig. 4(b), it can be observed that the TPDABCYΔ configuration can operate under soft–switching mode in the whole range of I_2 and for the following interval of $d : \frac{1}{2} \leqslant d \leqslant \frac{2}{3}$. In the case of the TPDABCΔY configuration, the soft–switching interval corresponds to $d : \frac{3}{2} \leqslant d \leq 2$.

The soft–switching operation regions for the four TPDABC configurations analyzed in this paper are validated by simulation. The parameters of the simulated converter are: $V_1 = 1$ p.u, $V_2 = 1.8$ p.u, $f = 20$ kHz, $L_{YY} = 0.89$ μH.

Fig. 5 shows the transformer voltages and currents, transistor and diode currents for one phase of the bridges and the output average current waveforms for each configuration, whose operating point corresponds to the mark depicted in Fig. 4, given by $I_2 = 0.4$ p.u. and $d = 1.8$.

Table 5 indicates that the converter operates under soft switching mode in both bridges when the anti–parallel diode is conducting when the transistor turn–on signal is activated. Thus, by analyzing the results of Fig. 5, it can be concluded that TPDABCYY, TPDABCΔΔ and TPDABCYΔ operate under hard–switching mode, while TPDABCΔY operates under soft–switching mode in both bridges. These results are in close agreement with the operating regions derived above.

Comparison and discussion of the results

In order to compare the performance of the different TPDABC configurations analyzed in this paper, shown in Fig. 3 and Fig. 4, Table 7 presents a comparative summary of the analytical results, represented by the factors of merit defined in this work.

Table 7
Comparisons between configurations of the TPDABC.

Configuration	Operation Mode	ΣIT_{rms}	VA_{Rating}	ΣIT_{rms}	$\sum I_{sw}$	Soft switching
TPDABCYY	Boost	2	1	2	2	1
	Unitary	3	3	3	2	2
	Buck	1	2	2	2	1
TPDABCΔΔ	Boost	3	3	2	2	1
	Unitary	4	3	3	2	2
	Buck	3	2	2	2	1
TPDABCYΔ	Boost	1	1	1	1	1
	Unitary	1	1	1	1	1
	Buck	4	4	4	4	4[†]
TPDABCΔY	Boost	4	4	4	4	4[‡]
	Unitary	1	1	1	1	1
	Buck	1	1	1	1	1

Score: Most unfavorable (1) to most favorable (4). [†] $(\frac{1}{2} \leqslant d \leqslant \frac{2}{3})$. [‡] $(\frac{3}{2} \leqslant d \leqslant 2)$.

In the first column of Table 7, the different configurations of TPDABC have been arranged, in the second column their different modes of operation, while in the first row the different factors of merit, mentioned above, have been arranged.

A valuation, between 1 and 4, has been established for each mode of operation and configurations, depending on the factors of merit defined in this paper. The highest valuation, 4, was assigned to the mode of operation and configuration which presents the best factor of merit. On the other hand, the minimum value, 1, was assigned to the mode of operation and configuration which presents the worst factor of merit.

Analyzing the valuations from the third to the sixth column of Table 7, it can be concluded that the star-delta and delta-star configurations present the maximum values for the Buck and Boost modes, respectively.

In addition, as already mentioned in Fig. 4, the TPDABCYΔ and TPDABCΔY configurations operating in Buck and Boost modes, respectively, can operate under soft–switching mode in the full range of the average output currents and for the range of variation of the voltage conversion ratio determined in Section "Determinat ion of soft–switching operation regions". This is represented in the seventh column of Table 7 with a valuation equal to 4, which corresponds to the maximum valuation, for these two configurations.

It is important to note that when the TPDABC converter operates bidirectionally, it can work in one direction in Buck mode and in the other one in Boost mode, being able to operate under soft-switching mode in both directions using TPDABCYΔ or TPDABCΔY configurations, respectively.

According to the results presented in Table 7, it can be concluded that the TPDABCYΔ and TPDABCΔY configurations are the most convenient options, even when the voltage conversion ratio varies within a certain range.

Conclusions

The operation of the Three–Phase Dual Active Bridge Converters (TPDABC) was analyzed and compared for different configurations that arise from using transformers with different types of connections: star–star, delta–delta, star–delta and delta–star.

Factors of merit were proposed and calculated to assess the different modes of operation for each configuration analyzed in this paper. These factors allow a relative assessment of losses in power semiconductors and transformer windings as well as the volume size of transformers.

From the analysis carried out, it can be concluded that for the same average power transferred by the converter, there are lower power losses in the semiconductors, lower losses in the transformer windings and a lower transformer volume size is required in the case of the Three–Phase Dual Active Bridge Converter whit star–delta connection (TPDABYΔ) when it operates in buck mode, for a wide range of average output current. The same occurs when the converter operates in boost mode for the case of the Three–Phase Dual Active Bridge Converter whit delta–star connection (TPDABΔY).

In addition, the limits of the soft–switching regions were determined, for each configuration, as function of the average output current and voltage conversion ratio. From these results it was concluded that both bridges of the TPDABC can operate under soft–switching mode over the entire range of average output current when the voltage conversion ratio is in the region defined by $\frac{1}{2} \leqslant d \leqslant \frac{3}{2}$ for the TPDABYΔ configuration, and $\frac{3}{2} \leqslant d \leqslant 2$ for the TPDABΔY configuration. On the other hand, it has been shown that the Three–Phase Dual Active Bridge Converter whit star–star and delta–delta connections can operate under soft–switching mode in the full operating range only when $d = 1$.

The above results allow the selection of the most convenient transformer connection for each application. Therefore, when there is a need to adapt two dc busbars with different voltage values, transferring power bidirectionally, with minimum power losses with a lower transformer volume size, over a wide range of power and allowing a certain range of variation in the voltage conversion ratio, it is more convenient to use the TPDABYΔ or TPDABΔY configurations, properly designing the transformer turns ratio.

Acknowledgments

This work was supported by National Council of Scientific and Technical Research (CONICET), National University of Río Cuarto (UNRC) and National University of Misiones (UNaM), Argentina.

References

[1] Hatziargyriou N, Asano H, Iravani R, Marnay C. Microgrids, power and energy magazine. IEEE 2007;5(4):78–94.
[2] Katiraei F, Iravani R, Hatziargyriou N, Dimeas A. Microgrids, power and energy magazine. IEEE 2008;6(3):54–65.
[3] Dursun E, Kilic O. Comparative evaluation of different power management strategies of a stand-alone pv/wind/pemfc hybrid power system. Int J Electr Power Energy Syst 2012;34(1):81–9.
[4] Haimin T, Kotsopoulos A, Duarte JL, Hendrix MAM. Transformer-coupled multiport zvs bidirectional dc–dc converter with wide input range. IEEE Trans on, Power Electr 2008;23(2):771–81.
[5] Baars NH, Everts J, Huisman H, Duarte JL, Lomonova EA. A 80 kw isolated dc–dc converter for railway applications. IEEE Trans Power Electr 2015(99). 1–1.
[6] Bizon N. Energy efficiency of multiport power converters used in plug-in/v2g fuel cell vehicles. Appl. Energy 2012;96:431–43. http://dx.doi.org/10.1016/j.apenergy.2012.02.075. URLhttp://www.sciencedirect.com/science/article/pii/S0306261912001766.
[7] Biao Z, Qiang S, Wenhua L, Yi X. Next-generation multi-functional modular intelligent ups system for smart grid. IEEE Trans Indust Electr 2013;60(9):3602–18.
[8] Tan X, Li Q, Wang H. Advances and trends of energy storage technology in microgrid. Int J Electr Power Energy Syst 2013;44(1):179–91. http://dx.doi.org/10.1016/j.ijepes.2012.07.015. URLhttp://www.sciencedirect.com/science/article/pii/S0142061512003754.
[9] Inoue S, Akagi H. A bidirectional isolated dc and dc converter as a core circuit of the next-generation medium-voltage power conversion system. IEEE Trans Power Electron 2007;22(2):535–42.
[10] Kumar L, Jain S. A multiple source dc/dc converter topology. Int J Electr Power Energy Syst 2013;51:278–91. http://dx.doi.org/10.1016/j.ijepes.2013.02.020. URLhttp://www.sciencedirect.com/science/article/pii/S014206151300080X.
[11] Duarte JL, Hendrix M, Simoes MG. Three-port bidirectional converter for hybrid fuel cell systems. IEEE Trans Power Electr 2007;22(2):480–7.
[12] Piris-Botalla L, Oggier GG, Airabella AM, García GO. Power losses evaluation of a bidirectional three-port dc/dc converter for hybrid electric system. Int J Electr Power Energy Syst 2014;58(0):1–8.
[13] Kheraluwala MN, Gascoigne RW, Divan DM, Baumann ED. Performance characterization of a high-power dual active bridge dc-to-dc converter. IEEE Trans Indust Appl 1992;28(6):1294–301.
[14] De Doncker RWAA, Divan DM, Kheraluwala MH. A three-phase soft-switched high-power-density dc/dc converter for high-power applications. IEEE Trans, Indust Appl 1991;27(1):63–73.
[15] Tao H, Kotsopoulos A, Duarte J, Hendrix MAM, A soft-switched three-port bidirectional converter for fuel cell and supercapacitor applications, In: Power Electronics Specialists Conference, 2005. PESC '05. IEEE 36th, 2005, pp. 2487–2493.
[16] Oggier GG, García GO, Oliva AR. Switching control strategy to minimize dual active bridge converter losses. IEEE Trans Power Electr 2009;24(7):1826–38.
[17] Rongyuan L, Pottharst A, Frohleke N, Bocker J. Analysis and design of improved isolated full-bridge bidirectional dc–dc converter, In: Power Electronics Specialists Conference, 2004. PESC 04. 2004 IEEE 35th Annual, Vol. 1, 2004, pp. 521–526 Vol.1.
[18] Krismer F, Round S, Kolar JW. Performance optimization of a high current dual active bridge with a wide operating voltage range, In: Power Electronics Specialists Conference, 2006. PESC '06. 37th IEEE, 2006, pp. 1–7.
[19] Oggier GG, García GO, Oliva AR. Modulation strategy to operate the dual active bridge dc–dc converter under soft switching in the whole operating range. IEEE Trans. Power Electron. 2011;26(4):1228–36.
[20] Naayagi RT, Forsyth AJ, Shuttleworth R. Bidirectional control of a dual active bridge dc–dc converter for aerospace applications. IET, Power Electron 2012;5(7):1104–18.
[21] Seunghun B, Dutta S, Bhattacharya S. Characterization of a three-phase dual active bridge dc/dc converter in wye-delta connection for a high frequency and high power applications, In: Energy Conversion Congress and Exposition (ECCE), 2011 IEEE, 2011, pp. 4183–4188.

[22] Mirzahosseini R, Tahami F. A phase-shift three-phase bidirectional series resonant dc/dc converter, In: IECON 2011 - 37th Annual Conference on IEEE Industrial Electronics Society, 2011, pp. 1137–1143.
[23] Molina JM, Garcia O, Asensi R, Alou P, Oliver JA, Cobos JA. Adaptive control for zvs three phase full active bridge converter with arcn, in: IEEE- Applied Power Electronics Conference and Exposition (APEC), Twenty-Seventh Annual, 2012, pp. 1324–1330.
[24] Xuan Z, Shenghua H, Guoyun N. A three-phase dual active bridge bidirectional zvs dc/dc converter. Phys Proc 24, Part A 2012(0):139–48.
[25] van Hoek H, Neubert M, De Doncker RW. Enhanced modulation strategy for a three-phase dual active bridge-boosting efficiency of an electric vehicle IEEE converter. Trans Power Electron 2013;28(12):5499–507.
[26] van Hoek H, Neubert M, Kroeber A, De Doncker RW. Comparison of a single-phase and a three-phase dual active bridge with low-voltage, high-current output, In: Renewable Energy Research and Applications (ICRERA), 2012 International Conference on, 2012, pp. 1–6.
[27] Segaran D, Holmes DG, McGrath BP. Comparative analysis of single and three-phase dual active bridge bidirectional dc–dc converters, In: Power Engineering Conference, 2008. AUPEC '08. Australasian Universities, 2008, pp. 1–6.
[28] Núñez RO, Oggier GG, Botterón F, García GO, Convertidor cc-cc con puentes duales activos trifásicos: Comparación transformador yy y dd, In: IEEE-Biennial Congress of Argentina (ARGENCON), San Carlos de Bariloche, Río Negro, Argentina, 2014, pp. 332–337. doi:http://dx.doi.org/10.1109/argencon.2014.6868515.
[29] Núñez RO, Oggier GG, Botterón F, García GO. Convertidor cc-cc con puentes duales activos trifásicos: Comparación transformador yy y yd, In: XXIV Congreso Argentino de Control Automático (AADECA), Buenos Aires, Argentina, 2014.
[30] Núñez RO, Oggier RO, Botterón F, García GO. Convertidor cc-cc con puentes duales activos trifásicos: Comparación transformador yy y dy, In: XVI Reunión de Trabajo en Procesamiento de la Información y Control (RPIC), Córdoba, Argentina, 2015.
[31] Jin K, Liu C. A novel pwm high voltage conversion ratio bidirectional three-phase dc/dc converter with yd connected transformer. IEEE Trans. Power Electron. 2016;31(1):81–8. http://dx.doi.org/10.1109/TPEL.2015.2397455.
[32] Baars NH, Everts J, Wijnands CGE, Lomonova EA. Performance evaluation of a three-phase dual active bridge dc-dc converter with different transformer winding configurations. IEEE Trans. Power Electron. 2016;31(10):6814–23. http://dx.doi.org/10.1109/TPEL.2015.2506703.
[33] Paice DA. Power Electronic Converter Harmonics. Multipulse Methods For Clean Power. New York, U.S.A.: Institute of Electrical and Electronics Engineers; 1996.
[34] W. Arendt, N. Nicolai, W. Tursky, R. Tobias, Application Manual Power Semiconductors, SEMIKRON International GmbH, Ilmenau. Germany, 2015.
[35] Rashid MH. Power electronics handbook. 2nd Ed. United States of America: Elsevier; 2007.